

Comparing ImageNet Pre-training with Digital Pathology Foundation Models for Whole Slide Image-Based Survival Analysis

Kleanthis Marios Papadopoulos¹, Tania Stathaki¹, Nazim Benzerdje^{2,3}, and Panagiotis Barmpoutis¹

¹ Imperial College London, Department of Electrical and Electronic Engineering,
London, UK
kp4718@ic.ac.uk

² Department of Pathology, Institut de Pathologie Multisite, Groupement Hospitalier
Sud, Lyon University Hospital, Pierre-Bénite, France

³ University of Lyon, Université Claude Bernard Lyon 1, Lyon, France

Abstract. The abundance of information present in Whole Slide Images (WSIs) renders them an essential tool for survival analysis. Several Multiple Instance Learning frameworks proposed for this task utilize a ResNet50 backbone pre-trained on natural images. By leveraging recently released histopathological foundation models such as UNI and Hibou, the predictive prowess of existing MIL networks can be enhanced. Furthermore, deploying an ensemble of digital pathology foundation models yields higher baseline accuracy, although the benefits appear to diminish with more complex MIL architectures. Our code will be made publicly available upon acceptance.

Keywords: Multiple Instance Learning · Whole Slide Images · Model Ensembles · Digital Pathology · Foundation Models.

1 Introduction

Whole Slide Images (WSIs) are obtained from the digitization of histopathological glass slides and are considered the main image modality in the field of digital pathology [1]. Digital pathology employs computational techniques to analyze whole slide images (WSIs) for various tasks, including cancer classification, tumor subtyping and survival analysis [1]. In clinical settings, survival analysis methods estimate the time until the occurrence of a significant event, such as death or disease recurrence.

Traditional survival analysis techniques, including Cox proportional hazards and Kaplan-Meier models, leverage handcrafted clinical features to estimate patients' Overall Survival (OS) time [2]. In contrast, deep learning enables automated feature extraction, prompting a shift toward techniques that leverage unstructured image features.

Zhu et al. present DeepConvSurv in [3], which is the first work to exploit the high information density of WSIs by proposing a Convolutional Neural Network (CNN) architecture for OS estimation.

Given that WSIs are gigapixel-size images, it is not feasible to directly train neural networks on them. Instead, WSIs are divided into smaller patches which can be processed individually by the network. In addition, challenges such as limited data availability and the lack of detailed annotations render Multiple Instance Learning (MIL) a popular approach for WSI-based survival analysis. A large number of works in this field use a ResNet50 backbone pre-trained on the ImageNet dataset to produce a feature map and subsequently employ a feature aggregation mechanism in accordance with the MIL framework.

Progress in the computer vision field is recently driven by Self-Supervised Learning (SSL) on large-scale datasets. SSL operates by leveraging unlabeled data to learn robust visual representations through pretext without relying on manual annotations [4]. SSL models are first pre-trained on these pretext tasks to capture general features and can then be fine-tuned on downstream tasks, allowing them to effectively adapt to specific applications [4]. These pre-trained models are also referred to as foundation models.

This development has inspired the release of several digital pathology foundation models, which are pre-trained on a vast number of unannotated WSIs found in public and private databases. These foundation models are considered a viable alternative to the ResNet50 backbone given their pre-training on pathology datasets instead of natural images.

This manuscript aims to provide a comprehensive comparison of the performance of Multiple Instance Learning (MIL)-based survival analysis networks using ResNet50 and two popular digital pathology foundation models. Furthermore, the use of a combination of feature extractors is explored to determine their impact on the accuracy of downstream MIL networks.

2 Related Work

2.1 Multiple Instance Learning

Multiple Instance Learning (MIL) is a Weakly Supervised Learning paradigm widely adopted in WSI workflows. In a typical binary classification problem, a sequence of images $X = \{X_1, X_2, \dots, X_N\}$ are used to train a network that can predict a label $y_k \in \{0, 1\}$, for $k = \{1, 2, \dots, N\}$. However, in the case of MIL, each image X_i is a bag composed of a sequence of M instances denoted by $X_i = \{x_{i1}, x_{i2}, \dots, x_{iM}\}$. A label is provided for the bag, but individual instances remain unlabeled. The standard MIL assumption is that individual instances are statistically independent from each other and that their ordering does not affect the MIL algorithm's operation. This problem formulation can be extended to multi-class classification and survival analysis. There exist two approaches for tackling MIL problems:

1. Instance-level approach: Each instance is assigned a score by a neural network and these scores are subsequently pooled [5].

2. Embedding-level approach: Bag instances are converted into compact embeddings providing a matrix of embeddings for each bag. MIL pooling is subsequently used for the downstream task [6].

The latter approach is often preferred as it avoids introducing further bias into the classification network [6]. Following feature extraction, a number of MIL aggregation mechanisms can be applied. Mean-pooling and max-pooling are the earliest aggregation techniques introduced, laying the groundwork for further experimentation [7]. Subsequent architectures such as TransMIL [8] leverage the ViT architecture and others introduce approaches to alleviate the high computational load associated with training ViTs. Examples include S4MIL and MambaMIL[9].

2.2 Digital Pathology Foundation Models

SSL models are typically trained on vast unlabeled datasets using pretext tasks, enabling them to learn robust visual representations [4]. After this pre-training phase, these models are fine-tuned on smaller labeled datasets that have been collected for a specific task in mind [4]. This approach has had great success in Natural Language Processing and has now become established in Computer Vision. Examples of pretext tasks include predicting objects' rotation angle and predicting missing image patches [4].

The most popular backbone choices for pretext tasks include ResNet variants and Vision Transformers (ViTs) [4]. Among SSL frameworks, iBOT and DINOV2 have become prominent for ViT pre-training because of their effectiveness in learning high-quality visual features. The iBOT framework employs a masked auto-encoder approach by training models to predict masked-out patches in images [10]. This helps the ViT backbone learn contextual relationships, a challenge typically faced by ViTs. DINOV2 utilizes a different learning strategy known as self-distillation [11]. In this approach, the model learns by comparing and aligning its representations across augmented views of the same image, enabling it to capture semantic features without reliance on labeled data [11].

The success of the DINOV2 network in particular has motivated the release of several foundation models in the digital pathology domain. Recently released cases include the UNI model [12] by Mahmood Lab and the Hibou family of models [13] by HistAI. The UNI model was pre-trained on the Mass-100K dataset, which consists of over 100,000 Formalin-Fixed, Paraffin-Embedded (FFPE) Hematoxylin and Eosin (H&E) WSIs collected from Massachusetts General Hospital (MGH) and Brigham and Women's Hospital (BWH), as well as external slides from the GTEx consortium [12]. This curated dataset does not include images from publicly available databases such as The Cancer Genome Atlas (TCGA). The pre-training process mimics the steps followed to produce DINOV2 [12].

DINOV2 with Registers enhances the original DINOV2 by introducing additional tokens, otherwise known as registers, to mitigate artifacts in ViT attention maps [14]. The Hibou model family adopts this framework for model training.

Similarly to UNI, HistAI’s models were pre-trained on a private dataset of approximately 1 million images [13]. This collection of images includes non H&E and cytology slides [13].

3 Methodology

We tackle survival analysis as a weakly supervised slide-level task in this work and we adopt the MIL convention of fine-tuning a number of MIL frameworks following WSI feature extraction from backbone models. We utilize the Clustering-constrained Attention Multiple Instance Learning (CLAM) framework [15] to separate tissue content from background, segment WSIs into patches, and convert them into feature representations. We use the ResNet50 backbone as a baseline and also extract features using UNI and the Hibou-Base checkpoint made publicly available by HistAI. We subsequently train a number of downstream MIL frameworks including MeanMIL [16], MaxMIL [16], ABMIL [7], and TransMIL [8]. We summarize our approach in Figure 1.

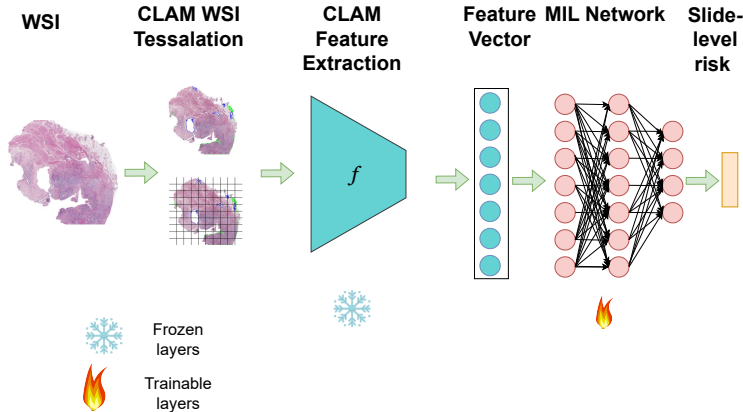


Fig. 1. Overview of single backbone training strategy

In addition, we explore foundation model ensembles based on tile embeddings through feature concatenation. A feature extractor f_i transforms a given WSI X_k into a feature matrix $\mathbf{F}_k \in \mathbb{R}^{m_k \times d}$, where m_k denotes the number of segmented patches for the k^{th} WSI and d denotes the embedding space dimension. We therefore obtain a feature representation \mathbb{G} mathematically defined as:

$$\mathbb{G} = \begin{bmatrix} \mathbb{F}_1 \\ \mathbb{F}_2 \\ \vdots \\ \mathbb{F}_N \end{bmatrix}, \quad (1)$$

where \mathbb{F}_i for $i = 1, \dots, N$ denotes the i^{th} feature matrix.

Following feature extraction, a trainable downstream MIL mechanism h converts the feature map into a slide-level risk prediction \hat{r} :

$$\hat{r} = h(\mathbb{G}) \quad (2)$$

We provide a graphical summary of this ensemble approach in Figure 2.

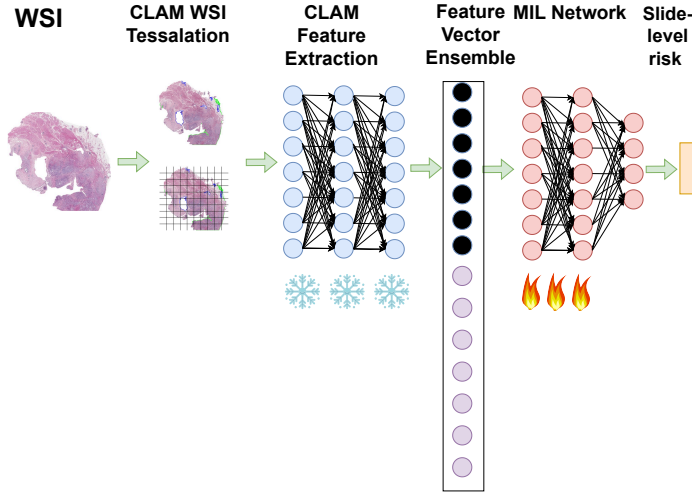


Fig. 2. Overview of feature extractor ensemble training strategy

4 Experiments & Results

4.1 Datasets

We use WSIs from the publicly available TCGA database, and specifically the Bladder Urothelial Carcinoma (BLCA), the Lung Adenocarcinoma (LUAD), and the Breast Invasive Carcinoma (BRCA) cohorts. We select FFPE H&E diagnostic slides for each cohort and we follow the convention of using one WSI per patient by selecting slides having "DX1" in their TCGA identifier. According to the TCGA documentation, the "DX" label denotes a diagnostic slide. A large number of patients have multiple "DX" slides but not all. This selection process yields $N = 373$, $N = 443$ and $N = 1061$ WSIs for BLCA, LUAD, and BRCA respectively. Survival analysis datasets comprise both censored and uncensored observations. Uncensored observations correspond to patients with known survival

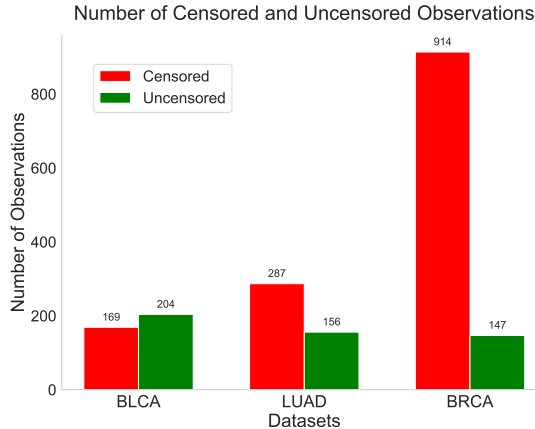


Fig. 3. Distribution of censored and uncensored patients in each TCGA dataset

times, while censored observations pertain to patients for whom survival time is not recorded, often because the patient was alive at the time of analysis. Figure 3 illustrates the distribution the distribution of censored and uncensored patients across each dataset, with the proportion of censored patients to the total number of patients being approximately 45% for the BLCA, 65% for the LUAD and 86% for the BRCA dataset respectively.

4.2 Implementation Details

Table 1 lists the dimension of the feature vector produced by each backbone along with the total number of parameters used during the pre-training phase. The same information for all model ensembles is provided in Table 2. We use the Negative Log Likelihood (NLL) as a bag-level loss function to train the aforementioned MIL networks and the concordance index to assess their prognostic accuracy. The number of trainable parameters for every MIL method is provided in Table A.1 in Appendix A. We divide the TCGA cohorts into train and validation sets and we report the results after applying K -fold cross validation ($K = 5$).

Our codebase is inspired by the MambaMIL framework [9], and we build upon its publicly available implementation. The project is implemented in PyTorch, and our code repository can be found at <https://github.com/MarioPaps/WSI-Survival-Analysis-ImageNet-vs-Digital-Pathology-Backbones.git>.

For training, we use the Adam optimizer and we set the batch size equal to 1 because the number of patches extracted for each WSI varies. We therefore perform backpropagation using gradient accumulation with the number of steps set to 32. Furthermore, we leverage early stopping and regularization to combat overfitting.

Feature Extractor	Dimension	Number of Parameters
ResNet50	1024	25,557,032 $\approx 25.6M$
UNI	1024	303,350,784 $\approx 303M$
Hibou-Base	768	8,5741,056 $\approx 8.6M$

Table 1. Dimensions of feature extractors used in the study

Ensemble Combination	Embedding Dimension
ResNet50 + UNI	2048
Hibou-Base + ResNet50	1792
Hibou-Base + UNI	1792
ResNet50 + UNI + Hibou-Base	2816

Table 2. Embedding Dimensions of the ensembles

4.3 Results

We report the 5-fold validation results by listing the concordance index and the standard deviation for every TCGA cohort in Table 3. We also list the concordance index values achieved by 2 model ensembles, ResNet50 with UNI and UNI with Hibou-Base, in Table 4.

MIL Method	BLCA	LUAD	BRCA	Average
ResNet50				
MeanMIL [16]	0.536 ± 0.072	0.580 ± 0.021	0.567 ± 0.061	0.561 ± 0.063
MaxMIL [16]	0.543 ± 0.044	0.596 ± 0.044	0.570 ± 0.049	0.570 ± 0.056
ABMIL [7]	0.570 ± 0.069	0.594 ± 0.031	0.565 ± 0.040	0.576 ± 0.061
TransMIL [8]	0.528 ± 0.049	0.597 ± 0.063	0.591 ± 0.053	0.560 ± 0.051
UNI				
MeanMIL [16]	0.570 ± 0.05	0.603 ± 0.030	0.597 ± 0.085	0.590 ± 0.073
MaxMIL [16]	0.530 ± 0.042	0.625 ± 0.076	0.610 ± 0.092	0.588 ± 0.089
ABMIL [7]	0.601 ± 0.046	0.605 ± 0.061	0.616 ± 0.066	0.607 ± 0.071
TransMIL [8]	0.565 ± 0.014	0.602 ± 0.047	0.628 ± 0.053	0.598 ± 0.051
Hibou-Base				
MeanMIL [16]	0.572 ± 0.036	0.614 ± 0.073	0.575 ± 0.089	0.587 ± 0.085
MaxMIL [16]	0.518 ± 0.031	0.605 ± 0.073	0.550 ± 0.080	0.558 ± 0.080
ABMIL [7]	0.570 ± 0.043	0.565 ± 0.080	0.617 ± 0.085	0.584 ± 0.088
TransMIL [8]	0.542 ± 0.053	0.611 ± 0.034	0.557 ± 0.045	0.570 ± 0.055

Table 3. Concordance index values for different MIL methods across TCGA cohorts

MIL Method	BLCA	LUAD	BRCA	Average
ResNet50+UNI				
MeanMIL [16]	0.591 \pm 0.028	0.586 \pm 0.064	0.581 \pm 0.080	0.586 \pm 0.075
MaxMIL [16]	0.527 \pm 0.050	0.603 \pm 0.049	0.585 \pm 0.089	0.572 \pm 0.080
ABMIL [7]	0.596 \pm 0.034	0.600 \pm 0.083	0.606 \pm 0.063	0.601 \pm 0.078
TransMIL [8]	0.580 \pm 0.033	0.589 \pm 0.050	0.600 \pm 0.078	0.590 \pm 0.070
UNI+Hibou-Base				
MeanMIL [16]	0.615 \pm 0.020	0.601 \pm 0.059	0.634 \pm 0.068	0.617 \pm 0.065
MaxMIL [16]	0.544 \pm 0.050	0.615 \pm 0.032	0.616 \pm 0.069	0.592 \pm 0.064
ABMIL [7]	0.587 \pm 0.026	0.623 \pm 0.063	0.610 \pm 0.008	0.607 \pm 0.049
TransMIL [8]	0.551 \pm 0.025	0.578 \pm 0.060	0.608 \pm 0.058	0.579 \pm 0.062
ResNet50+Hibou-Base				
MeanMIL [16]	0.603 \pm 0.020	0.605 \pm 0.058	0.656 \pm 0.080	0.621 \pm 0.071
MaxMIL [16]	0.530 \pm 0.034	0.592 \pm 0.046	0.563 \pm 0.064	0.562 \pm 0.061
ABMIL [7]	0.579 \pm 0.034	0.604 \pm 0.089	0.655 \pm 0.078	0.613 \pm 0.087
TransMIL [8]	0.561 \pm 0.021	0.599 \pm 0.050	0.643 \pm 0.057	0.601 \pm 0.056
ResNet50 + UNI + Hibou-Base				
MeanMIL [16]	0.603 \pm 0.022	0.595 \pm 0.079	0.650 \pm 0.074	0.616 \pm 0.078
MaxMIL [16]	0.525 \pm 0.044	0.603 \pm 0.049	0.570 \pm 0.063	0.566 \pm 0.064
ABMIL [7]	0.598 \pm 0.022	0.604 \pm 0.096	0.644 \pm 0.058	0.615 \pm 0.081
TransMIL [8]	0.563 \pm 0.036	0.590 \pm 0.040	0.609 \pm 0.053	0.616 \pm 0.078

Table 4. Concordance index values for feature ensembles of MIL methods across TCGA cohorts

5 Conclusions

The results in Table 3 indicate that both histopathological feature extractors can consistently enhance the predictive prowess of the MIL networks used in this study. In most cases, the UNI backbone achieves a larger improvement over ResNet50 compared to Hibou-Base.

The reported concordance index values in Table 4 demonstrate that a significant performance improvement can be obtained by utilizing an ensemble of feature extractors. This improvement is particularly pronounced with the two simpler MIL architectures, which are MeanMIL [16] and MaxMIL [16]. Despite the ensemble of ResNet50 and UNI having a larger embedding dimension, the combinations of Hibou-Base with ResNet50 and UNI deliver more frequent improvements in outcome prediction accuracy. Furthermore, while combining two histopathological feature extractors typically results in a higher concordance index, mixing a feature extractor pre-trained on ImageNet with one pre-trained on WSIs outperforms the dual histopathological extractor approach in some cases. Lastly, the ensemble of all three feature extractors does not appear to yield a notable performance improvement in any MIL architecture.

Future work includes incorporating feature extractors pre-trained using different SSL approaches, besides self-distillation employed in DINOv2, to further assess the effect of different strategies on prognostic accuracy.

6 Acknowledgments

We acknowledge computational resources and support provided by the Imperial College Research Computing Service (<http://doi.org/10.14469/hpc/2232>).

Appendix A: MIL Model Parameters

Table A.1 presents the number of trainable parameters for MeanMIL [16], MaxMIL [16], ABMIL [7], and TransMIL [8], assuming an input embedding dimension of 1024.

MIL Network Number of Parameters	
MeanMIL [16]	526,852 $\approx 527K$
MaxMIL [16]	526,852 $\approx 527K$
ABMIL [7]	592,645 $\approx 593K$
TransMIL [8]	2,673,172 $\approx 2.7M$

Table A.1. Trainable parameter counts for MIL networks with an input embedding dimension of 1024.

Appendix B: Hyperparameter Choices

Table B.1 summarizes the hyperparameter choices that are consistently applied across all model setups.

Table B.1. Hyperparameter options common across all model configurations

Datasets	BLCA	LUAD	BRCA
Number of WSIs	373	443	1061
Batch size	1	1	1
Gradient accumulation steps	32	32	32
Optimizer	Adam	Adam	Adam
Bag weight	0.7	0.7	0.7
Learning rate	$2e-4$	$1e-4$	$5e-5$
Epochs	200	200	200
Early stopping	Enabled	Enabled	Enabled
Earliest stop epoch	40	40	40
L1 regularization	$1e-4$	$1e-4$	$1e-4$
Patience epochs	10	5	10
Dropout rate	0.25	0.25	0.25
Weight decay	$1e-3$	$5e-4$	$5e-4$

References

1. J. Van der Laak, G. Litjens, and F. Ciompi, “Deep learning in histopathology: the path to the clinic,” *Nature Medicine*, vol. 27, no. 5, pp. 775–784, 2021.
2. T. Qaiser, C.-Y. Lee, M. Vandenberghe, J. Yeh, M. Gavrielides, J. Hipp, M. Scott, and J. Reischl, “Usability of deep learning and he images predict disease outcome-emerging tool to optimize clinical trials,” *npj Precision Oncology*, vol. 6, p. 37, 06 2022.
3. X. Zhu, J. Yao, and J. Huang, “Deep convolutional neural network for survival analysis with pathological images,” in *2016 IEEE International Conference on Bioinformatics and Biomedicine (BIBM)*, (China, Shenzhen), pp. 544–547, December 2016.
4. D. Hendrycks, M. Mazeika, S. Kadavath, and D. Song, “Using self-supervised learning can improve model robustness and uncertainty,” *Advances in neural information processing systems*, vol. 32, 2019.
5. G. Liu, J. Wu, and Z.-H. Zhou, “Key instance detection in multi-instance learning,” in *Asian conference on machine learning*, pp. 253–268, PMLR, 2012.
6. X. Wang, Y. Yan, P. Tang, X. Bai, and W. Liu, “Revisiting multiple instance neural networks,” *Pattern Recognition*, vol. 74, pp. 15–24, 2018.
7. M. Ilse, J. Tomczak, and M. Welling, “Attention-based deep multiple instance learning,” in *Proceedings of the 35th International Conference on Machine Learning* (J. Dy and A. Krause, eds.), vol. 80 of *Proceedings of Machine Learning Research*, pp. 2127–2136, PMLR, 10–15 Jul 2018.
8. Z. Shao, H. Bian, Y. Chen, Y. Wang, J. Zhang, X. Ji, and y. zhang, “Transmil: Transformer based correlated multiple instance learning for whole slide image classification,” in *Advances in Neural Information Processing Systems* (M. Ranzato, A. Beygelzimer, Y. Dauphin, P. Liang, and J. W. Vaughan, eds.), vol. 34, pp. 2136–2147, Curran Associates, Inc., 2021.
9. S. "Yang, Y. Wang, and H. Chen, “"mambamil: Enhancing long sequence modeling with sequence reordering in computational pathology"”, in *"Medical Image Computing and Computer Assisted Intervention – MICCAI 2024"*, (Cham), pp. 296–306, Springer Nature Switzerland, 2024.
10. J. Zhou, C. Wei, H. Wang, W. Shen, C. Xie, A. Yuille, and T. Kong, “ibot: Image bert pre-training with online tokenizer,” 2022.
11. M. Oquab, T. Darcet, T. Moutakanni, H. Vo, M. Szafraniec, V. Khalidov, P. Fernandez, D. Haziza, F. Massa, A. El-Nouby, M. Assran, N. Ballas, W. Galuba, R. Howes, P.-Y. Huang, S.-W. Li, I. Misra, M. Rabbat, V. Sharma, G. Synnaeve, H. Xu, H. Jegou, J. Mairal, P. Labatut, A. Joulin, and P. Bojanowski, “Dinov2: Learning robust visual features without supervision,” 2024.
12. R. J. Chen, T. Ding, M. Y. Lu, D. F. K. Williamson, G. Jaume, A. H. Song, B. Chen, A. Zhang, D. Shao, M. Shaban, M. Williams, L. Oldenburg, L. L. Weishaupt, J. J. Wang, A. Vaidya, L. P. Le, G. Gerber, S. Sahai, W. Williams, and F. Mahmood, “"towards a general-purpose foundation model for computational pathology"”, *Nature Medicine*, vol. 30, pp. 850–862, mar 2024.
13. D. Nechaev, A. Pchelnikov, and E. Ivanova, “Hibou: A family of foundational vision transformers for pathology,” 2024.
14. T. Darcet, M. Oquab, J. Mairal, and P. Bojanowski, “Vision transformers need registers,” in *The Twelfth International Conference on Learning Representations*, 2024.

15. M. Y. Lu, D. F. Williamson, T. Y. Chen, R. J. Chen, M. Barbieri, and F. Mahmood, “"data-efficient and weakly supervised computational pathology on whole-slide images",” *Nature Biomedical Engineering*, vol. 5, no. 6, pp. 555–570, 2021.
16. M. U. Oner, J. M. S. Kye-Jet, H. K. Lee, and W.-K. Sung, “Studying the effect of mil pooling filters on mil tasks,” 2020.